Absence of hyperplasia in Gasp-1 overexpressing mice is dependent on myostatin up-regulation

Caroline Brun, Luce Périé, Fabienne F. Baraige, Barbara Vernus, Anne Bonnieu, Véronique V. Blanquet

Cellular Physiology and Biochemistry

Cell Physiol Biochem 2014;34:1241-1259
DOI: 10.1159/000366335
Published online: September 29, 2014
Accepted: August 11, 2014

1421-9778/14/0344-1241$39.50/0

Original Paper

Absence of Hyperplasia in *Gasp-1* Overexpressing Mice is Dependent on Myostatin Up-Regulation

Caroline Brun[a] Luce Périé[a] Fabienne Baraige[a] Barbara Vernus[b] Anne Bonnieu[b] Véronique Blanquet[a]

[a]INRA, UMR 1061 Génétique Moléculaire Animale, Université de Limoges, FR 3503 GEIST, Faculté des Sciences et Techniques, Limoges, [b]INRA, UMR 866 Dynamique Musculaire et Métabolisme, Université Montpellier 1, Montpellier, France

Key Words
Muscle development • Hypertrophy • Hyperplasia • Satellite cells • GASP-1 • Myostatin • Pax7 • Smad2/3 • Akt • Erk1/2

Abstract
Background/Aims: Overexpression of *Gasp-1*, an inhibitor of myostatin, leads to a hypermuscular phenotype due to hypertrophy rather than hyperplasia in mice. However to date, the cellular and molecular mechanisms underlying this phenotype are not investigated. ***Methods:*** Skeletal muscles of overexpressing *Gasp-1* mice, called *Tg(Gasp-1)* mice, were analyzed by histological methods. Satellite cell-derived myoblasts from these mice were used to investigate the molecular mechanisms. ***Results:*** We demonstrated that hypertrophy in *Tg(Gasp-1)* mice was related to a myonuclear accretion during the first 3 postnatal weeks and an activation of the pro-hypertrophic Akt/mTORC/p70S6K signaling. In accordance with these results, we showed that overexpressing *Gasp-1* primary myoblasts proliferated faster and myonuclei average per myotube was increased during differentiation. Molecular analysis revealed that *Gasp-1* overexpression resulted in increased myostatin expression related to its auto-regulation. Despite its inhibition, myostatin led to Pax7 deregulation through its non-canonical Erk1/2 signaling pathway. Consistent with this, inhibition of Erk1/2 signaling pathway as well as neutralization of secreted myostatin rescue the Pax7 expression in overexpressing *Gasp-1* myoblasts. ***Conclusion:*** Our study shows that myostatin is able to act independently of its canonical pathway to regulate the Pax7 expression. Altogether, our results indicate that myostatin could regulate muscle development despite its protein inhibition.

Pr. Véronique Blanquet

Institut National de Recherche Agronomique, UMR 1061, Génétique Moléculaire Animale, 123, avenue Albert Thomas, 87060 Limoges Cedex (France)
Tel. +33 5 55 45 76 64, Fax +33 5 55 45 76 53, E-Mail veronique.blanquet@unilim.fr

Introduction

Skeletal muscle is composed of heterogeneous populations of muscle fibers bundled together and which differ in their metabolism and contractile properties [1, 2]. This type of organization confers to skeletal muscles remarkable levels of plasticity in the face of changing external conditions. During embryonic development, the number of myofibers and their size increase until birth [3]. Postnatal muscle growth is then achieved by hypertrophy of myofibers in mouse and can be divided into two distinct steps. Between birth and 3 weeks old, hypertrophy is supported by a rapid increase in the number of myonuclei within the myofiber *via* activation and fusion of satellite cells (myonuclear accretion) [4]. Then, satellite cells enter in quiescence and reach their adult level around the third week [5]. From 3 weeks old to adulthood, muscle mass regulation is dependent of protein synthesis mainly and the myofiber hypertrophy occurs without addition of new nuclei. During the past two decades, much progress has been made in unraveling the molecular mechanisms underlying either adult muscular hypertrophy (increase in myofiber size) or atrophy (decrease in myofiber size) [6, 7]. The maintenance of the muscle homeostasis is finely regulated by the balance between protein synthesis and protein degradation. This protein turnover is induced in response to various stimuli such as exercise, inactivity or environmental factors (hypoxia, heat, nutrient availability, growth factors) [7]. Among these growth factors, the myostatin (Mstn), a member of the transforming growth factor-β (TGF-β) superfamily, is the most potent inhibitor of skeletal muscle mass [8, 9].

Disruption of the *Mstn* gene in mice leads to a dramatic increase in skeletal muscle mass due to both hyperplasia and hypertrophy, and to an overall glycolytic muscle phenotype [8, 10]. Moreover, Mstn-null mice (*Mstn* $^{-/-}$) have a reduced adipogenesis and their organ weights are lower [11]. Naturally occurring mutations in *Mstn* gene lead to a hypermuscular phenotype in several species, from mice to human [8, 12-15].

Interestingly, the action of this growth factor on muscle mass is not restricted to the embryonic period, as myostatin is also able to regulate adult muscle growth and size. Mice carrying a postnatal deletion of the *myostatin* gene or adult mice injected with various inhibitors of myostatin exhibit also an increased muscle mass resulting only from hypertrophy, suggesting that myostatin regulates hyperplasia during embryonic development [16-19].

After binding to the activin receptor type IIB (ActRIIB), myostatin acts through its canonical Smad2/3 pathway to inhibit myoblast proliferation by up-regulation of p21 [20], and differentiation by inhibition of MyoD and myogenin [21]. The phosphorylation of Smad2/3 also reduces the Akt/mTOR/p70S6K protein synthesis pathway [22, 23]. Myostatin is able to act independently of Smad2/3 *via* the mitogen-activated protein kinase (MAPK) pathway such as the extracellular signal-regulated kinase (Erk) 1/2 pathway leading to the down-regulation of Pax7 [24, 25]. Notably, other members of TGF-β superfamily such as activin A or GDF-11 can bind to ActRIIB and stimulate the same intracellular signaling pathway [26].

Various myostatin-binding proteins have been identified that are able of inhibiting myostatin activity [27]. Among them, GASP-1 (growth and differentiation factor-associated serum protein-1) is a secreted glycoprotein that contains protease inhibitor domains such as the tandem Kunitz domains that are unique among the related myostatin-binding proteins, the follistatin domain and the netrin domain, which allow GASP-1 to bind both mature myostatin and myostatin propeptide respectively and thus inhibit myostatin activity [28-30]. It was also shown that GASP-1 exhibits a relatively high affinity for BMP-2, BMP-4 and TGF-β1 [31]. However, these interactions do not necessarily lead to inhibition of their signaling pathway. Only, the myostatin or GDF-11 signal transduction is inhibited by this interaction, suggesting an additional role for GASP-1 as a carrier protein. As we have recently shown, overexpressing *Gasp-1* transgenic mice (called *Tg(Gasp-1)*) present an increased muscle mass due to myofiber hypertrophy rather than hyperplasia. No variation in fiber type proportions was observed. Furthermore, body fat deposition was not altered in the *Tg(Gasp-1)* mice [32]. All these data suggest that *Gasp-1* overexpression has no effect on

myostatin during prenatal muscle development. Body weight increase in *Tg(Gasp-1)* mice is visible at the third week of postnatal life and remains stable throughout adulthood, showing that *Gasp-1* overexpression leads to the muscular fiber hypertrophy mainly during the first 21 days after birth and would later participate to skeletal muscle mass maintenance.

To investigate the cellular and molecular mechanisms regulating muscle mass in *Tg(Gasp-1)* mice, we examined the proliferation and differentiation capabilities in satellite cell-derived myoblasts from *Tg(Gasp-1)* mouse line compared to wild-type and *Mstn* $^{-/-}$ myoblasts. As observed in *Mstn* $^{-/-}$ cells, we showed that *Tg(Gasp-1)* myoblasts increase the Akt/mTORC/p70S6K signaling, enhancing myoblast differentiation and myotube size by protein synthesis. Moreover, we showed an increased number of myonuclei per myofiber in *Tg(Gasp-1)* skeletal muscle confirming a higher myonuclear accretion contributing to the muscle hypertrophy. Molecular analysis revealed a myostatin up-regulation associated to a Pax7 down-regulation through Erk1/2 signaling pathway. We demonstrated that this *myostatin* up-regulation counteracts *Gasp-1* effect during embryonic muscle development leading to the absence of hyperplasia. At last, we showed that overexpression of an inhibitor of a TGF-β superfamily member leads to a global deregulation of these members and their related proteins.

Materials and Methods

Animals

Mstn $^{-/-}$ mice, harboring a constitutive deletion of the third *Mstn* exon, and *Tg(Gasp-1)* mice, overexpressing *Gasp-1* ubiquitously, have been described previously [16, 32]. All mice were bred and housed in the animal facility of Limoges University under controlled specific pathogen free conditions (21°C, 12-h light/12-h dark cycle) with free access to standard mouse chow and tap water. All of the experimental procedures were carried out in accordance with the recommendations in the guidelines of the European Communities Council (Directive 2010/63/UE). Experiments were approved by the Committee on the Ethics of Animal Experiments of the Author's Institution, "Comité Régional d'Ethique de l'Expérimentation Animale" of the Limousin region (n°17-2013-17).

Isolation of satellite cell-derived myoblasts and cell culture

Primary myoblasts were obtained using mice between 4 and 6 weeks of age. Concisely, murine myoblasts were isolated from hind limb muscles after enzymatic digestion by pronase. Cells were plated at a density of 20,000 cells/cm2 on Matrigel®-coated Petri dishes (BD Biosciences) in Ham's F10 supplemented with 20% horse serum and 1% penicillin/streptomycin. Cells were maintained at 37°C in a water-saturated atmosphere containing 5% CO2 in air for 2 days. Then, cells were washed with Ham's F10 (Gibco) and placed in complete growth medium supplemented with 5 ng/ml basic fibroblast growth factor (bFGF, Invitrogen), 20% horse serum and 1% penicillin/streptomycin (Growth Medium, GM). The myoblast population was enriched by differential adhesion compared with fibroblasts by serial 30-min preplate procedures after trypsinization. To induce differentiation (0 h of differentiation), primary myoblasts were reached at 80% confluence and switched in Differentiation Medium (DM) consisting of Ham's F10 containing 15% horse serum and 1% penicillin/streptomycin.

Myoblasts were treated with a recombinant myostatin protein (788-G8-010/CF, R&D Systems) at the final concentration of 250 ng/ml or with the same amounts of 4 mM HCl as control for 16 h. For Erk1/2 pathway inhibition, cells were pre-treated for 2 h with 5, 10 or 20 μM of a selective ERK inhibitor FR180204 (R&D Systems) or with the same amounts of DMSO as control. For myostatin neutralizing, cells were incubated with a goat anti-myostatin antibody (sc-6884, Santa Cruz) at different concentrations (2.5 to 10 μg/ml) for 16 h or with the same amounts of an isotype control (normal goat IgG, sc-2028, Santa Cruz).

Proliferation assay and measurement of myogenic index

Primary myoblast proliferation was assessed as described previously [33]. Cells were seeded at 2,500 cells per well in GM in 96-well microtiter plates and fixed at regular 24 h periods, before the Methylene Blue staining. Absorbance at 590 nm was read using an ELISA plate reader. Fusion index was determined

as the ratio of the nuclei number in the cells containing two or more nuclei to the total nuclei number in hematoxylin-stained primary myotubes. Cells were stained with hematoxylin/eosin as previously described [29].

RNA extraction, reverse transcription, and gene expression analysis

Total RNA from cells at each kinetic point and from embryos and skeletal muscles of wild-type and *Tg(Gasp-1)* was obtained by anion exchange chromatography (RNeasy mini Kit, Qiagen Inc). The High Capacity cDNA Archive Kit (Applied Biosystems) was used to convert 2 µg of total RNA into single-stranded cDNA. Taqman primers and probe sets used in this study were as follows: 18S (Hs99999901_s1), Gapdh (Mm99999915_g1), Gasp-1 (Mm00725281_m1), myostatin (Mm03024050_m1). Quantitative PCR reaction was performed from 20 ng of cDNA in an ABI Prism 7900HT Sequence Detection System (Applied Biosystems) using 40 cycles of 95°C for 15 sec followed by 60°C for 1 min. Relative mRNA expression values were calculated by the ΔΔCt method with normalization of each sample to the average change in cycle threshold value of the controls. TLDA (Taqman low density array, Applied Biosystems) assays were performed based on the same above conditions, except from each sample, 200 ng cDNA were used per TLDA card. Two TLDA cards were used: in the first one, the 93 selected target genes involved in myogenesis were described previously [32]; in the second one, the 43 selected genes involved in TGF-β signaling pathway were listed in the Table 2. Each card features five control assays: 18S, Gapdh, Tbp (Mm00446973_m1), Dffa (Mm00438410_m1) and Fcgrt (Mm00438887_m1).

Enzyme-linked immunosorbent assay (ELISA) of GASP-1 and myostatin

Cell supernatants were concentrated by centrifugation at 3,000 × g with Amicon Ultra-15 Centrifugal Filter Unit with Ultracel-3 membrane (Millipore). GASP-1 concentrations from concentrated cell supernatants or mouse plasmas were determined in a sandwich ELISA (GASP-1 DuoSet ELISA kit, R&D Systems), as described previously [29]. Myostatin concentrations were also determined in a sandwich ELISA (GDF-8/Myostatin Quantikine ELISA kit, R&D Systems). Following the manufacturer recommendation, the propeptide was removed from myostatin by an acid activation followed by neutralization. The final dilutions measured for concentrated cell supernatants or mouse plasmas were 1:10 and 1:40 respectively. All measurements were performed in triplicate and data for the standard curve were fitted to a logistic plot with the MARS Data Analysis Software (BMG Labtech) to determine the levels of GASP-1 or myostatin.

Proteome profiler arrays

To investigate the pathways by which GASP-1 enhances myogenesis, we performed a determination of phospho-kinase and apoptosis-related proteins using Proteome Profiler Arrays (Human Apoptosis Array, Human Phospho-Kinase Array, Human Phospho-MAPK Array, R&D Systems), according to the manufacturer's instructions. Briefly, the cells were collected, rinsed in 1× PBS and lysed in lysis buffer. The arrays were incubated overnight with the diluted lysates (300 µg) at 4°C on a rocking platform shaker. The blots were detected using an enhanced chemiluminescence (BM Chemiluminescence Western Blotting Substrate (POD)) (Roche Applied Science) and exposed to a film (GE Healthcare Hyperfilm ECL, GE Healthcare). Densitometric analysis of the array image files were performed using ImageQuant TL software (GE Healthcare).

Protein extraction and immunoblotting

Cells and mouse tissues were collected by centrifugation (12,000 × g, 4°C, 20 min) and then lysed in a RIPA buffer (50 mM Tris, pH 8, 150 mM NaCl, 0.1% SDS, 1% NP-40, 0.5% sodium deoxycholate, and protease inhibitors). Proteins were quantified at A595nm using the Bradford assay (Bio-Rad). Equal amounts of proteins (20-50 µg) were resolved on SDS-polyacrylamide gels (4-12% gradient, Invitrogen) and transferred onto 0.2 µm nitrocellulose membranes. Then, membranes were blocked using 5% non-fat dry milk (w/v) in TBST0.1% buffer (50 mM Tris-HCl, 150 mM NaCl, pH 7.4, 0.1% Tween-20) for 1 h at room temperature, followed by incubation with specific primary antibodies overnight at 4°C. The following primary antibodies were used for immunoblotting: 1:5000 dilution of anti-Akt antibody (MAB2055, R&D Systems), 1:500 dilution of anti-phospho-Akt antibody (AF887, R&D Systems), 1:400 dilution of anti-cdk2 (sc-6248, Santa Cruz), 1:400 dilution of anti-cyclinD1 (sc-8396, Santa Cruz), 1:1000 dilution of anti-Erk1/2 (AF1576, R&D Systems), 1:500 dilution of anti-phospho-Erk1/2 (MAB1018, R&D Systems), 1:2000 dilution

of anti-GAPDH (AF5718, R&D Systems), 1:1000 dilution of anti-GASP-1 (AF2070, R&D Systems), 1:4000 dilution of anti-MyHC (M4276, Sigma-Aldrich), 1:1000 dilution of anti-MyoD (M3512, Dako), 1:1000 dilution of anti- Myogenin (M3559, Dako), 1:2000 dilution of anti-Smad2/3 (AF3797, R&D Systems), 1:500 dilution of anti-phospho-Smad3 (AB3226, R&D Systems), 1:200 dilution of anti-p21 (sc-53870, Santa Cruz) and 1:1000 dilution of anti-β-actin (sc-1615, Santa Cruz). After four washes in TBST0.1%, membranes were incubated for 1 h at room temperature with 1:1000 dilution of secondary antibodies: anti-goat IgG Horseradish peroxidase (HRP) conjugate (P0449, Dako), anti-mouse IgG HRP conjugate (P0447, Dako), or anti-rabbit HRP conjugate (P0399, Dako). After four more washes in TBST0.1%, immunoblots were developed by enhanced chemiluminescence. The developed films were analyzed using ImageQuant TL software (GE Healthcare).

Immunofluorescence

Primary myoblasts were fixed in paraformaldehyde (PFA) 4%/PBS, washed three times in PBS, and permeabilized with HEPES/Triton X-100 buffer, pH7.4, consisting of 20 mM HEPES, 300 mM sucrose, 50 mM NaCl2, 3 mM MgCl2 and 0.5% Triton X-100. Dissected skeletal muscles were frozen in liquid nitrogen-cooled isopentane and stored at -80°C for further analysis or sectioned (8 µm thick) for immunostaining. Cryosections were thawed at room temperature and air-dried, fixed in PFA 4%/PBS, washed three times in PBS before permeabilization with cold methanol at -20°C and processed for antigen retrieval in 10 mM citrate buffer, pH 6 at 90°C for 2 × 5 min in a microwave. Then, cells and cryosections were blocked for 1 h in blocking buffer consisting of 10% goat serum, 1% bovine serum albumin (BSA) and 0.1% Triton X-100 in PBS, at room temperature. Incubation with primary antibodies diluted in BSA 1%/PBS took place overnight at 4°C. After three washes in BSA 0.2%/Tween-20 0.1%/PBS, slides were incubated for 15 min at 37°C with secondary antibodies conjugated to a fluorescent dye (Alexa Fluor® 488 Goat Anti-Mouse IgG (H+L) (A10680, Invitrogen) for anti-MyHC and anti-Pax7 or Alexa Fluor® 546 F(ab')2 Fragment of Goat Anti-Rabbit IgG (H+L) (A11071, Invitrogen) for anti-laminin and anti-MyoD) diluted in BSA 1%/PBS. The staining was completed with three washes in PBS and incubation for 5 min at room temperature in DAPI solution to label cell nuclei. Primary antibodies used for these analyses were as follows: anti-laminin (L9393, Sigma-Aldrich), anti-MyHC (M4276, Sigma-Aldrich), anti-MyoD (sc-304, Santa Cruz) and anti-Pax7 (DSHB). Images were acquired with a Leica DMI6000B inverted epifluorescence microscope using the MetaMorph software (Molecular Devices, Sunnyvale, USA). Myofiber cross-sectional areas were calculated from laminin-stained cryosections from randomly chosen fields using ImageJ software v1.43 (http://rsbweb.nih.gov/ij/). Myonuclei were manually counted in images captured at 40X magnification using the MetaMorph software to determine the number of myonuclei per fiber. Myonuclei were selected as they were located within the laminin boundary and as they are $Pax7^{-}$. MyoD/Pax7 cell populations were counted manually from 20 fields per experiments using the same software.

Results

Overexpression of Gasp-1 in mice has no effect during prenatal myogenesis

Tg(Gasp-1) mice have an overall increase in body weight as a result of an increase in muscle mass [32]. To confirm whether the muscle mass increase is due to hypertrophy rather than hyperplasia of all skeletal muscles, we performed histological analysis on two skeletal muscles of 12-week-old mice, *tibialis anterior* (TA) and *soleus*, which stand out for their fiber metabolism, glycolytic or oxidative respectively (Fig. 1A). Whatever muscle tested, no significant difference in muscle fiber number was observed between wild-type (WT) or *Tg(Gasp-1)* mice, underlying a lack of hyperplasia in contrast to the observed phenotype of $Mstn^{-/-}$ mice (Fig. 1C). However, *Tg(Gasp-1)* mice has an increased muscle fiber cross-sectional area (CSA) when compared to the WT mice, confirming that muscle mass increased is due to hypertrophy (Fig. 1D). As hypertrophy could be related to the addition of new nuclei from activated satellite cells within the myofiber and/or to the increased rate of protein synthesis, we analyzed the number of myonuclei per myofiber in TA and *soleus* skeletal muscles of 12-week-old mice. Satellite cell nuclei labelled by Pax7 were excluded from this counting and only myonuclei beneath the basal lamina labelled by laminin were

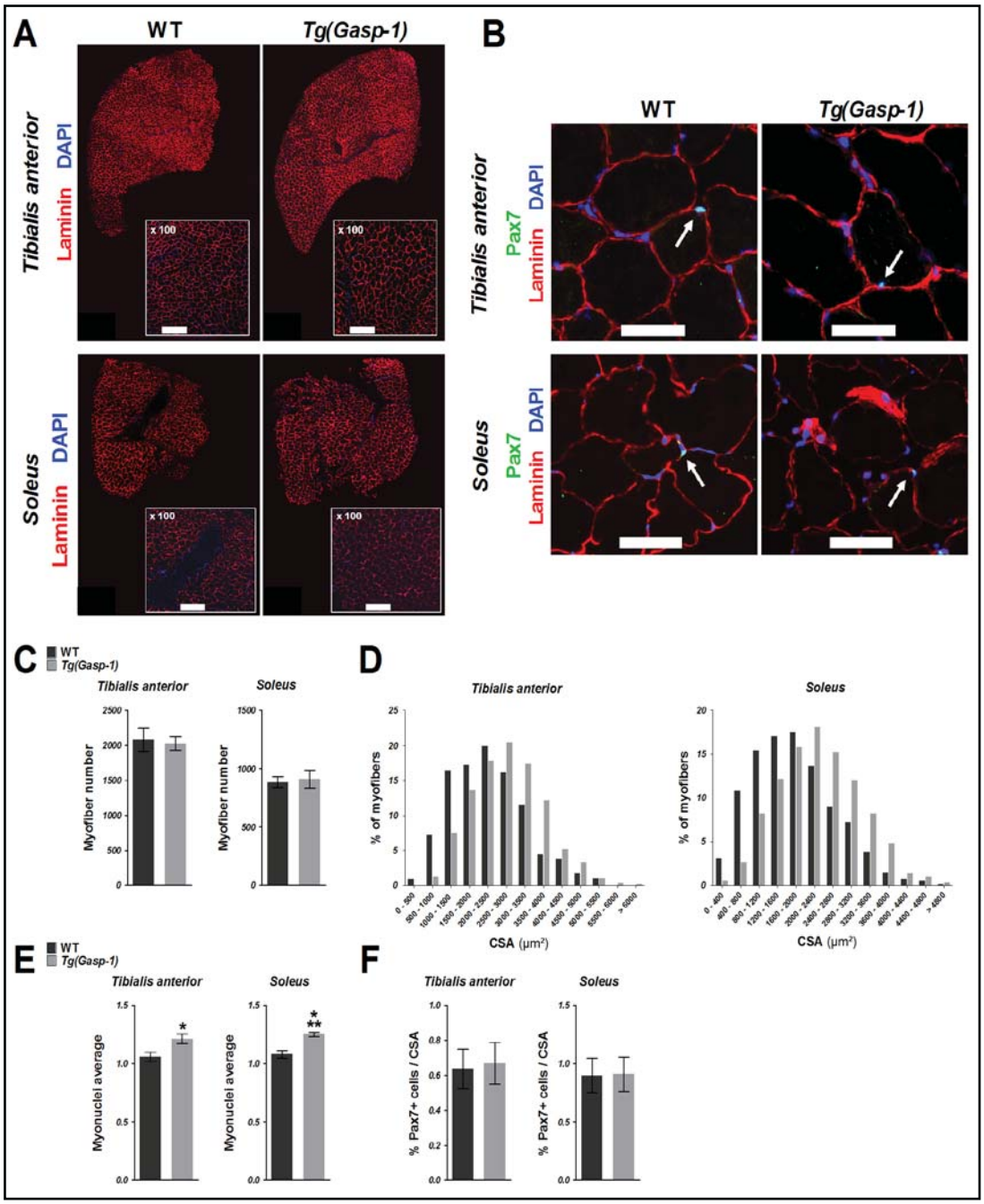

Fig. 1. Characterization of skeletal muscles from *Tg(Gasp-1)* mice. (A) Representative cryosections of *tibialis anterior* (TA) and *soleus* muscles from 12-week-old wild-type (WT) and *Tg(Gasp-1)* mice. Laminin (red) and DAPI (blue) staining showed basal lamina of myofibers and nuclei respectively. Scale bars, 250 µm. (B) Representative cryosections of TA and *soleus* muscles from 12-week-old WT and *Tg(Gasp-1)* mice immunostained for laminin (red), Pax7 (green) and DAPI (blue). Satellite cells (Pax7$^+$) are shown with white arrows. Scale bars, 50 µm. (C) Fiber number in TA and *soleus* from 12-week-old WT and *Tg(Gasp-1)* mice. *n = 3 mice/genotype.* Values are means ± SEM. (D) Frequency distribution of TA and *soleus* skeletal muscle fiber cross-sectional areas (CSA) between WT and *Tg(Gasp-1)* mice. *n = 3 mice/genotype.* (E) Quantification of the number of myonuclei per fiber in TA and *soleus* from 12-week-old WT and *Tg(Gasp-1)* mice. *n = 3 mice/genotype.* Values are means ± SEM. Statistical significance was assessed by a Student's t test analysis when compared with the WT. **: p value < 0.05 ; ***: p value < 0.001* (F) Percentage of satellite cells per cross-sectional area. *n = 3 mice/genotype.* Values are means ± SEM.

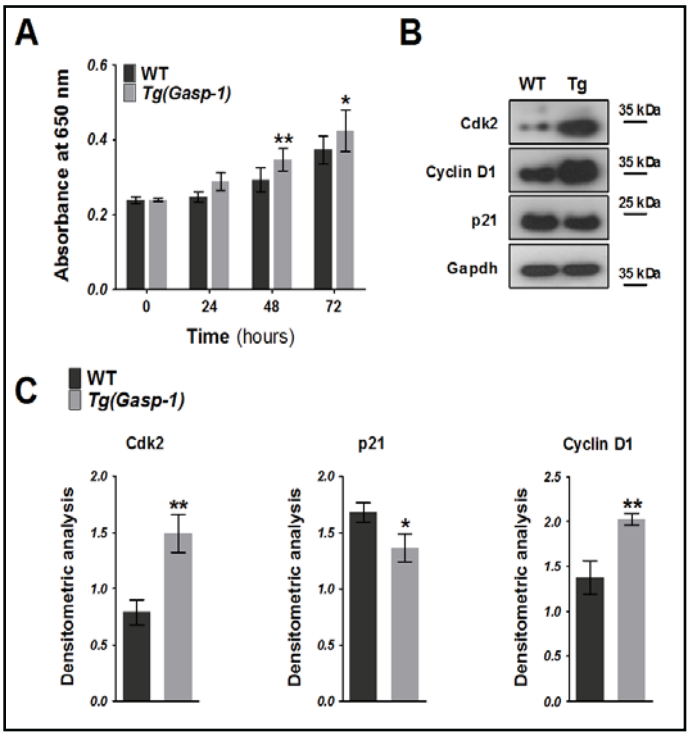

Fig. 2. Overexpression of *Gasp-1* in *Tg(Gasp-1)* primary myoblasts enhances cell proliferation. (A) Wild-type (WT) and *Tg(Gasp-1)* primary myoblasts were plated at 2,500 cells per well and grown in growth medium for a period of 72 h. Proliferation was measured by Methylene Blue assay. *n = 4 independent experiments*; values correspond to means ± SD. Statistical significance was assessed by a two-way ANOVA when compared with the WT. (B) Immunoblot analysis of cdk2, cyclin D1 and p21 expression of WT and *Tg(Gasp-1)* myoblasts grown under proliferating conditions for 24 h. Nitrocellulose membranes were also probed with anti-Gapdh antibody to show equal loading of samples. (C) Densitometric analysis of the relative levels of Cdk2, cyclin D1 and p21. These levels were normalized to Gapdh signals of three distinct experiments. Values are means ± SEM. Statistical significance was assessed by a Student's t test analysis when compared with the WT. **: p value < 0.05 ; **: p value < 0.01 .*

counted (Fig. 1B). We showed an increased number of myonuclei per myofiber in *Tg(Gasp-1)* skeletal muscle demonstrating a higher myonuclear accretion (Fig. 1E). We also compared the number of satellite cell ($Pax7^+$) into the cross-sections of *tibialis* and *soleus* skeletal muscles of 12-week-old mice. As shown in Fig. 1F, the number of satellite cells is unaffected in overexpressing *Gasp-1* skeletal muscles when compared to the WT, suggesting that GASP-1 promotes hypertrophy independently of the adult satellite cell pool. Thus, the increase of myonuclei number per myofiber seems to be related to an activation and fusion of satellite cells prior to the first 12 weeks of life.

Overexpression of Gasp-1 leads to an increased proliferation rate and an improved differentiation

To investigate the molecular mechanisms regulating muscle mass in *Tg(Gasp-1)* mice, myoblasts derived from *Tg(Gasp-1)* and wild-type WT satellite cells were compared *in vitro*. First, the proliferation rate was monitored during 72 hours and revealed that *Tg(Gasp-1)* myoblasts proliferated faster than the WT myoblasts (Fig. 2A). We also analyzed the expression of Cdks and their associated cyclins, especially Cyclin-dependent kinase 2 (Cdk2) and cyclin D1, which are known to positively regulate cell-cycle progression. Western blot analysis showed an increase of Cdk2 and cyclin D1 in *Tg(Gasp-1)* myoblasts compared to WT myoblasts, consistent with the increase of proliferation rate, while p21, a Cylin-dependent kinase inhibitor (CKI), decreased in *Tg(Gasp-1)* myoblasts (Fig. 2B and 2C). These results revealed that *Gasp-1* overexpression promoted cell-cycle progression.

To analyze the effect of *Gasp-1* overexpression during myoblast differentiation, fusion indexes of WT and *Tg(Gasp-1)* myotubes were determined. After 72 hours of differentiation, we observed that both WT and *Tg(Gasp-1)* myoblasts fused to form myotubes and *Tg(Gasp-1)* myotubes had a greater size (Fig. 3A). We showed that *Gasp-1* overexpression in myotubes led to an increase of differentiation when compared to the WT cells (Fig. 3B). Average numbers of mononuclei per myotube revealed that *Tg(Gasp-1)* myotubes had more myonuclei than WT myotubes, especially in late stages of differentiation, suggesting an increase of myoblast

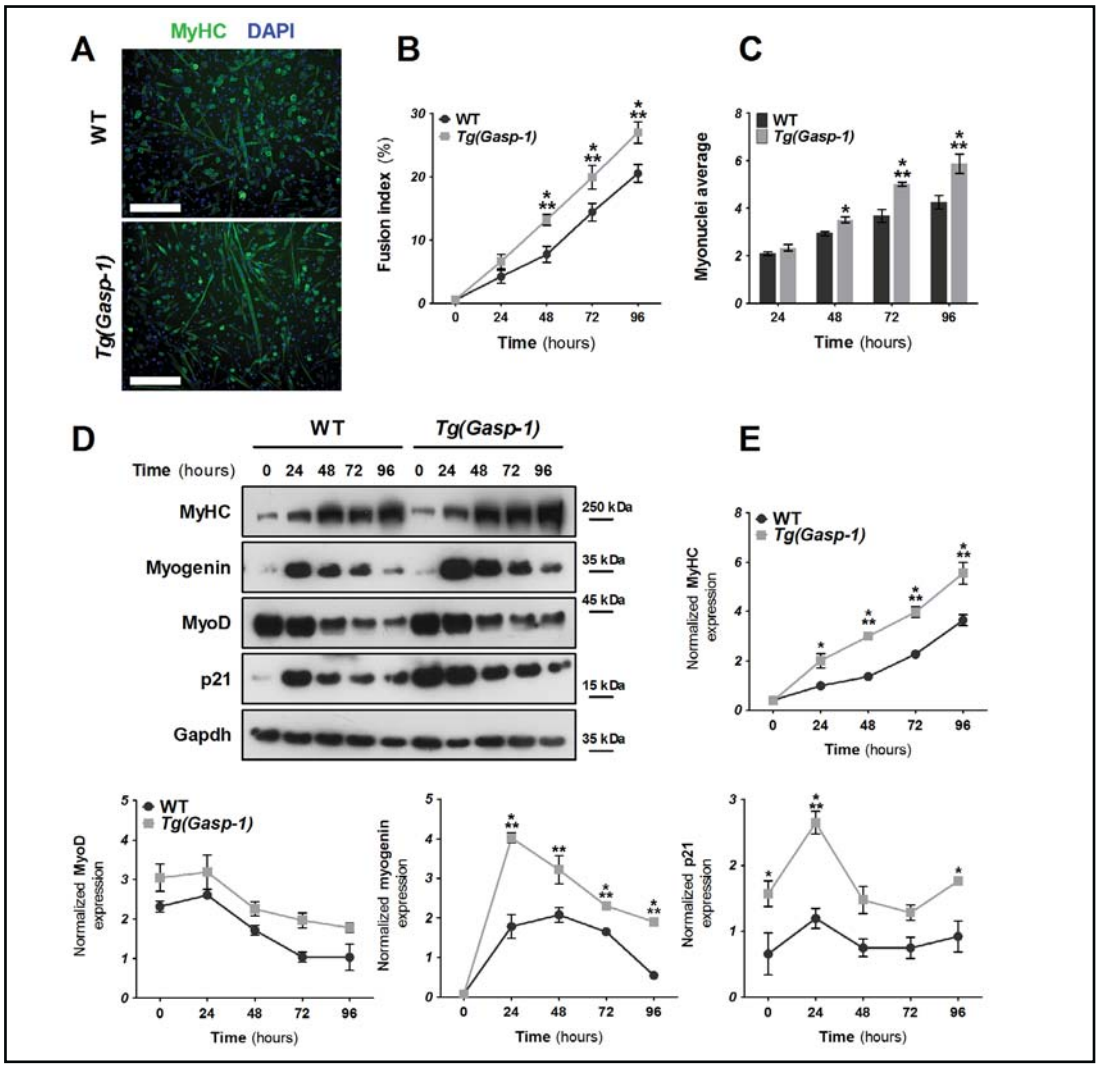

Fig. 3. Overexpression of *Gasp-1* enhances differentiation of *Tg(Gasp-1)* primary myoblasts. (A) Wild-type (WT) and *Tg(Gasp-1)* myotubes were immunostained for MyHC protein at 72 h after induction of differentiation. Scale bars, 100 µm. (B) Fusion indexes during 96 h of WT and *Tg(Gasp-1)* myoblast differentiation were determined from hematoxylin/eosin staining. *n = 3 independent experiments*; values are means ± SD. (C) Average numbers of myonuclei per WT or *Tg(Gasp-1)* myotubes at 24 h, 48 h, 72 h and 96 h. *n = 3 independent experiments*; values are means ± SD. (D) Immunoblot analysis of MyHC, myogenin, MyoD and p21 from 0 h to 96 h of differentiation in WT and *Tg(Gasp-1)* primary myotubes. Gapdh was analyzed to ensure equal loadings. (E) All graphs represent densitometric analysis of MyoD, myogenin, MyHC and p21 expressions normalized to Gapdh. Values are means ± SEM. Statistical significance was assessed by a two-way ANOVA when compared with the WT. **: p value < 0.05 ; **: p value < 0.01 ; ***: p value < 0.001.*

fusion (Fig. 3C). Consistent with this increase of differentiation, some gene expression results showed that the myogenic regulatory factors (MRFs), MyoD and myogenin, were up-regulated in the *Tg(Gasp-1)* myoblasts when compared to the WT cells, as well as p21 and MyHC all along the time course (Fig. 3D and 3E). All these results correlated to an increase of differentiation when *Gasp-1* is overexpressed.

Myostatin is up-regulated in Tg(Gasp-1) primary myoblasts and mice.

In order to further characterize the molecular basis for the observed improvement of myogenic processes, we performed an expression array analysis of 91 genes involved in

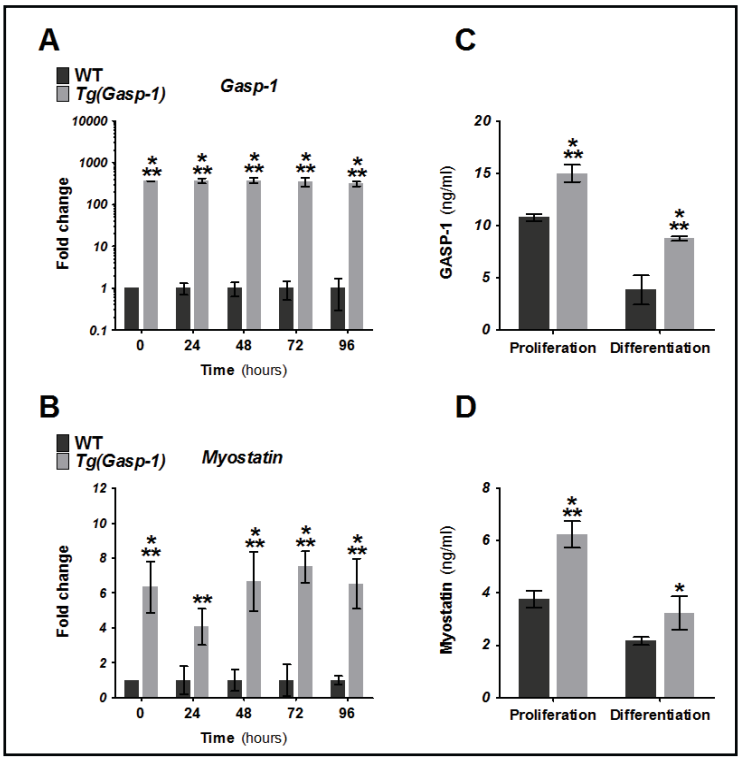

Fig. 4. *Tg(Gasp-1)* primary myoblasts overexpress myostatin. (A-B) Relative mRNA expression levels of *Gasp-1* and *myostatin* were measured by qRT-PCR from 0 h to 96 h of differentiation in wild-type (WT) and *Tg(Gasp-1)* primary myotubes. *n = 3 independent experiments*; graphs display fold changes ± SD. (C-D) Cells were cultured in growth medium (proliferation) or in differentiation medium (differentiation) for 48 h. Concentrations of GASP-1 and myostatin proteins secreted into culture media were determined in sandwich ELISA. (*n = 3 independent experiments*; values are means ± SD). Statistical significance was assessed by a Student's t test analysis when compared with the WT. **: p value < 0.05; **: p value < 0.01; ***: p value < 0.001.*

Table 1. Relative expression levels of deregulated genes in *Tg(Gasp-1)* myoblasts. List of up-regulated or down-regulated genes by more than 1.5-fold in *(Tg:Gasp-1)* primary myoblasts compared with wild-type primary myoblasts during proliferation. Statistical significance was assessed by a Student's t test analysis when compared with the WT. *n.s., non-significant ; *: p value < 0.05 ; **: p value < 0.01 ; ***: p value < 0.001*

	Gene ID	Symbol	Description	Fold changes	*p*-value
Up-regulated	278507	*Gasp-1*	Growth and differentiation factor associated serum protein-1	263.52	***
	17700	*Mstn*	Myostatin	2.61	***
	16324	*Inhbb*	Inhibin beta B chain	1.59	*
Down-regulated	18509	*Pax7*	Paired box protein 7	- 1.52	*
	83554	*Fstl3*	Follistatin like 3	- 1.52	*
	26420	*Mapk9*	Mitogen-activated protein kinase 9	- 1.53	*n.s.*
	66508	*Lamtor*	Late endosomal/lysosomal adaptor, MAPK and MTOR activator 1	- 1.58	*n.s.*
	14313	*Fst*	Follistatin	- 1.63	*
	17131	*Smad7*	Mothers against decapentaplegic homolog 7	- 1.67	*
	21803	*Tgfb1*	Transforming growth factor beta 1	- 1.84	*n.s.*
	18505	*Pax3*	Paired box protein 3	- 1.88	*n.s.*
	12156	*Bmp2*	Bone morphogenetic protein 2	- 1.93	**
	16000	*Igf1*	Insulin-like growth factor 1	- 2.68	*
	12159	*Bmp4*	Bone morphogenetic protein 4	- 4.95	***

muscle development during proliferation, 48 h after plating (*n = 5 independent experiments*). *Gasp-1* expression was increased more than 200-fold in the *Tg(Gasp-1)* myoblasts compared to the WT, confirming that *Gasp-1* overexpression was significant in *Tg(Gasp-1)* satellite cell-derived primary myoblasts (Table 1). We also found that *myostatin* and *Inhbb* (Inhibin beta B chain) were also up-regulated in *Tg(Gasp-1)* cells. In contrast, genes that have been previously described as components of myostatin pathway - *Fst* (follistatin), *Fstl3* (follistatin-like 3) and *Smad7* - were down-regulated in *Tg(Gasp-1)* myoblasts (Table 1). Interestingly, *Gasp-1* overexpression led to down-regulation of three TGF-β superfamily members - *Bmp4*,

		Gene ID	Symbol	Description	Assay	E9.5		E14.5		P15	
						FC	*p*-value	FC	*p*-value	FC	*p*-value
Members of TGF-β signaling pathway	TgF-β	21803	*Tgfb1*	Transforming growth factor β 1	Mm01178819_m1	-1.28	*n.s.*	-1.38	*	-1.06	*n.s.*
		21808	*Tgfb2*	Transforming growth factor β 2	Mm00436955_m1	1.29	*n.s.*	-1.14	*n.s.*	1.04	*n.s.*
		21809	*Tgfb3*	Transforming growth factor β 3	Mm00436960_m1	5.69	*n.s.*	-1.13	*n.s.*	1.56	*n.s.*
	Activins/Inhibins	16322	*Inha*	Inhibin alpha	Mm00439683_m1	3.09	*n.s.*	1.64	*n.s.*	-1.86	*n.s.*
		16323	*Inhba*	Inhibin beta-A	Mm00434339_m1	1.24	*n.s.*	1.09	*n.s.*	-1.04	*n.s.*
		16324	*Inhbb*	Inhibin beta-B	Mm01286587_m1	14.08	**	1.52	*	2.24	*n.s.*
		16325	*Inhbc*	Inhibin beta-C	Mm00439684_m1	N.D.	N.D.	N.D.	N.D.	N.D.	N.D.
		16326	*Inhbe*	Inhibin beta-E	Mm00434340_g1	N.D.	N.D.	N.D.	N.D.	N.D.	N.D.
		17700	*Mstn*	Myostatin	Mm01254559_m1	13.33	**	1.55	*	2.01	*
		14561	*Gdf11*	Growth differentiation factor 11	Mm01159973_m1	-6.02	*n.s.*	-1.01	*n.s.*	1.17	*n.s.*
		110075	*Bmp3*	Bone morphogenetic protein 3	Mm00557790_m1	2.13	*	1.31	*n.s.*	1.04	*n.s.*
		14560	*Gdf10*	Growth differentiation factor 10	Mm01220860_m1	3.37	*	-1.03	*n.s.*	1.34	*n.s.*
		12155	*Bmp15*	Bone morphogenetic protein 15	Mm00437797_m1	N.D.	N.D.	N.D.	N.D.	N.D.	N.D.
		14566	*Gdf9*	Growth differentiation factor 9	Mm00433565_m1	-1.49	*n.s.*	-1.04	*n.s.*	-9.18	*n.s.*
	BMP/GDF	18119	*Nodal*	Nodal	Mm00443040_m1	1.31	*n.s.*	1.69	*n.s.*	-1.16	*n.s.*
		12153	*Bmp1*	Bone morphogenetic protein 1	Mm00802220_m1	1.65	*n.s.*	-1.24	*n.s.*	-1.07	*n.s.*
		12156	*Bmp2*	Bone morphogenetic protein21	Mm01340178_m1	-1.15	*n.s.*	-1.13	*n.s.*	-1.25	*n.s.*
		12159	*Bmp4*	Bone morphogenetic protein 4	Mm01321704_m1	-4.79	*	-1.51	*	-1.82	**
		12162	*Bmp7*	Bone morphogenetic protein 7	Mm00432102_m1	-2.40	**	-1.05	*n.s.*	-1.27	*n.s.*
	IGF	16000	*Igf1*	Insulin-like growth factor 1	Mm01228180_m1	2.418	*	1.04	*n.s.*	1.40	*n.s.*
		16002	*Igf2*	Insulin-like growth factor 2	Mm00580426_m1	1.450	*n.s.*	-1.31	*n.s.*	-11.49	*
Inhibitors of TGF-β signaling pathway		215001	*Gasp-2*	Growth and differentiation factor-associated serum protein-2	Mm01308311_m1	-2.00	*	-2.05	*n.s.*	-2.17	*n.s.*
		278507	*Gasp-1*	Growth and differentiation factor-associated serum protein-1	Mm00725281_m1	19.69	**	21.10	*	56.04	***
		14313	*Fst*	Follistatin	Mm00514982_m1	-1.65	*	-1.20	*n.s.*	-1.15	*n.s.*
		83554	*Fstl3*	Flrg, follistatin like 3	Mm00473194_m1	-2.01	*	1.30	*n.s.*	-1.00	*n.s.*
		13179	*Dcn*	Decorin	Mm00514535_m1	3.71	**	1.22	*n.s.*	1.12	*n.s.*
		16998	*Ltbp3*	Latent TGF-b binding protein 3	Mm00521855_m1	3.25	*	1.16	*n.s.*	-1.29	*n.s.*
		268977	*Ltbp1*	Latent TGF-b binding protein 1	Mm00498255_m1	-1.48	*n.s.*	-1.34	*n.s.*	-1.05	*n.s.*
		108075	*Ltbp4*	Latent TGF-b binding protein 4	Mm00723631_m1	1.87	*	1.10	*n.s.*	-1.20	*n.s.*
		21667	*Tdgf1*	Cripto	Mm03024051_g1	N.D.	N.D.	N.D.	N.D.	N.D.	N.D.
		12111	*Bgn*	Biglycan	Mm01191753_m1	1.14	**	1.45	*n.s.*	1.13	*n.s.*
		18121	*Nog*	Noggin	Mm01297833_s1	1.50	*n.s.*	1.13	*n.s.*	1.26	*n.s.*
		12667	*Chrd*	Chordin	Mm00438203_m1	3.54	*	1.02	*n.s.*	-1.40	*n.s.*
		14314	*Fstl1*	Follistatin like 1	Mm00433371_m1	2.02	*n.s.*	1.22	*n.s.*	-1.39	*n.s.*
		29817	*Fstl2*	Igfbp7	Mm03807886_m1	4.99	*	1.04	*n.s.*	-1.38	*n.s.*
	MRF/Pax	17130	*Smad6*	SMAD family member 6	Mm00484738_m1	-3.64	*	1.08	*n.s.*	1.06	*n.s.*
		17131	*Smad7*	SMAD family member 7	Mm00484742_m1	-1.79	*	-1.03	*n.s.*	-1.31	*
		17877	*Myf5*	Myogenic factor 5	Mm00435125_m1	-1.33	*n.s.*	-1.12	*n.s.*	-2.25	*n.s.*
		17878	*Myf6*	Myogenic factor 6	Mm00435126_m1	2.77	*	1.79	*	1.65	*n.s.*
		17927	*Myod1*	Myogenic differentiation 1	Mm00440387_m1	6.30	**	1.12	*n.s.*	-1.05	*n.s.*
		17928	*Myog*	Myogenin	Mm00446194_m1	2.22	*	-1.07	*n.s.*	-2.04	*n.s.*
		18505	*Pax3*	Paired box protein 3	Mm00435493_m1	-3.50	**	-1.67	*	-2.17	*n.s.*
		18509	*Pax7*	Paired box protein 7	Mm00834079_m1	-2.66	*	-1.27	*n.s.*	-1.77	*

Table 2. List of 43 target genes selected for Taqman Low Density Array and their relative expression levels in Tg(Gasp-1) mice. Fold change (FC) of genes involved in the TGF-β signaling pathway in Tg(Gasp-1) mice are compared with wild-type mice at embryonic stages E9.5 and E14.5 and at post-natal day 15 (P15). Statistical significance was assessed by a Student's t test analysis when compared with the WT. n.s., non-significant ; *: p value < 0.05 ; **: p value < 0.01 ; ***: p value < 0.001

Bmp2 and *Tgfb1* - known to interact with GASP-1 which doesn't inhibit their signaling activity (Table 1) [31]. *Pax7* and *Pax3*, two transcription factors known to be involved in the regulation of skeletal muscle stem cells, were also down-regulated. Finally, we observed a decreased expression of *Igf-1* (insulin-like growth factor-1) known to have a pro-hypertrophic activity [34]. Since expression array analysis revealed an up-regulation of *myostatin* expression in overexpressing *Gasp-1* cells, we performed a qPCR of these two genes during the first 96 h of differentiation of *Tg(Gasp-1)* compared to the WT myotubes. As seen in Fig. 4A and 4B,

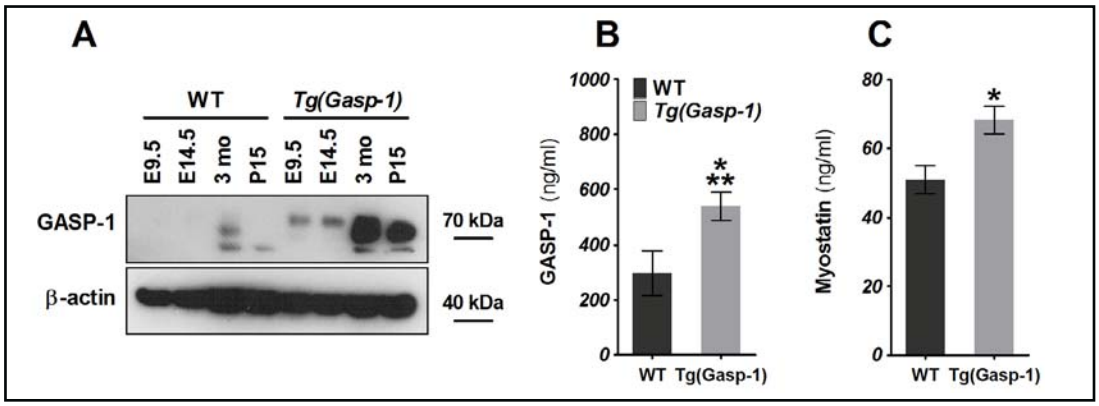

Fig. 5. *Tg(Gasp-1)* mice overexpress myostatin. (A) Immunoblot analysis of GASP-1 at E9.5, E14.5, P15 and 3 months (3 mo) of life in Wild-type (WT) and *Tg(Gasp-1)* mice. β-actin was analyzed to ensure equal loadings. (B-C) Quantification of GASP-1 and myostatin proteins from WT and *Tg(Gasp-1)* serum (*n = 6 mice/genotype*; values are means ± SD). Statistical significance was assessed by a Student's t test analysis when compared with the WT. **: p value < 0.05 ; **: p value < 0.01 ; ***: p value < 0.001.*

Gasp-1 and *myostatin* were stably up-regulated all along the time course. The ELISA provided the evidence that more GASP-1 and myostatin were found secreted from primary *Tg(Gasp-1)* myoblasts (Fig. 4C and 4D).

Since *Gasp-1* overexpression seems to deregulate expression of *myostatin* and TGF-β superfamily-related genes in *Tg(Gasp-1)* primary myoblasts, we investigated their expression levels at different steps of muscle growth during late embryonic starting at E9.5, fetal starting at E14.5 and at postnatal day 15 (P15) (Table 2) [35]. Similarly to primary myoblasts, *Bmp4*, *Bmp2*, *Tgfb1*, *Fst*, *Fstl3* and *Smad7* were down-regulated as *Pax3* and *Pax7* in *Tg(Gasp-1)* mice compared to the wild-type (Table 2). We also found an up-regulation of *Inhbb*, *Mstn* and *Gasp-1* (Table 2). Western blotting analysis of GASP-1 confirmed the protein overexpression at all the studied stages of mouse development (Fig. 5A). We also showed that GASP-1 protein and active mature form of myostatin were more secreted in *Tg(Gasp-1)* mice serum compared to the WT (Fig. 5B-C). This up-regulation of myostatin in *Tg(Gasp-1)* myoblasts, confirmed in mice, led us to analyze the signaling pathway activated in these cells.

ERK1/2 signaling pathway is activated in Tg(Gasp-1) primary myoblasts

To characterize the signaling pathways affected by *Gasp-1* overexpression in myoblasts, three types of microarrays directed against 84 phospho-proteins were used (Fig. 6A). Among them, 13 proteins were significantly affected as shown in Fig. 6B. *Gasp-1* overexpression increased the phosphorylation of Akt1 (S473) and Akt2 (S474) in agreement with the inhibition of myostatin pathway (Fig. 6B, positions 1-3). It also increased mTOR and p70S6 kinase activation in *Tg(Gasp-1)* myoblasts when compared to the WT cells, suggesting an overall increase in Akt/mTOR/p70S6K protein synthesis pathway (Fig. 6B, positions 7, 10). Heat shock proteins 27 and 70 (HSP27 and HSP70), which are known to prevent skeletal muscle atrophy [36, 37], were significantly more phosphorylated in *Tg(Gasp-1)* myoblasts as HSP60 (Fig. 6B, positions 4-6). Conversely, the phosphorylation of CKIs p21 and p27 had decreased in *Tg(Gasp-1)* myoblasts compared to the WT (Fig. 6B, positions 8-9). Surprisingly, the phosphorylation of Erk1/2 had increased in *Tg(Gasp-1)* primary myoblasts when compared to WT myoblasts (Fig. 6B, positions 11-13). To confirm that *Gasp-1* overexpression led to the inhibition of the canonical myostatin pathway in *Tg(Gasp-1)* primary myoblasts, the phosphorylation rate of Smad3 was assessed between WT, *Tg(Gasp-1)* and *Mstn* $^{-/-}$ myoblasts. Immunoblot analysis revealed a decrease of phospho-Smad3 in *Tg(Gasp-1)* and *Mstn* $^{-/-}$ compared to the WT, confirming the inhibition of the myostatin-induced activation of Smad2/3 signaling pathway (Fig. 6C and 6D). We also compared the Akt and Erk1/2 phosphorylation rates in WT, *Tg(Gasp-1)* and *Mstn* $^{-/-}$ myoblasts. Akt phosphorylation had

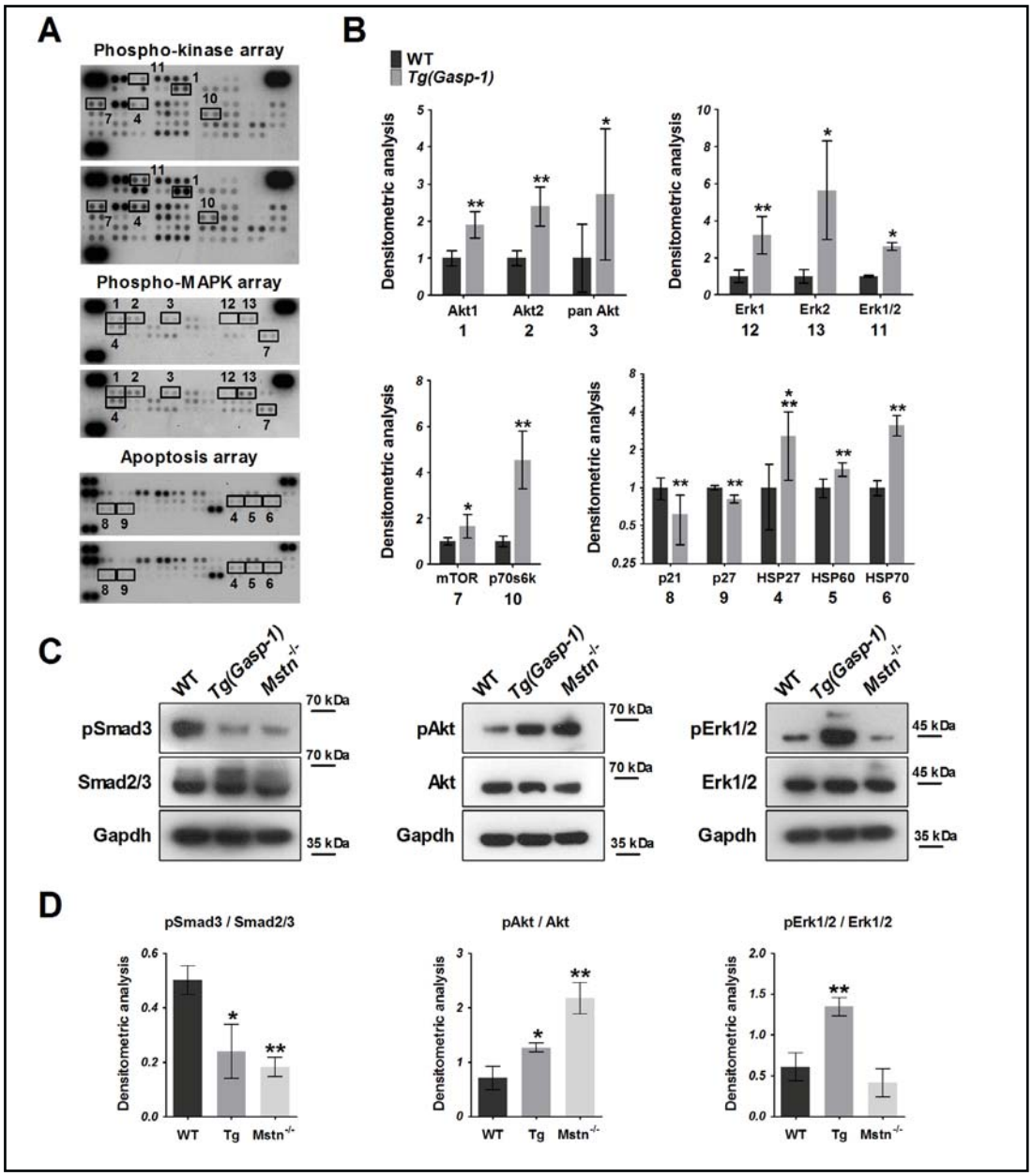

Fig. 6. Phospho-proteomic profiling of wild-type and *Tg(Gasp-1)* primary myoblasts. (A) Representative macroarray results and (B) densitometric analysis of phosphorylated signaling proteins in wild-type (WT) and *Tg(Gasp-1)* primary myoblasts under proliferating conditions with significant variations. *Tg(Gasp-1)* results (*n = 3 independent experiments*, means ± SEM) are expressed as ratios (*Tg(Gasp-1)* value/WT value). Statistical significance was performed using a two-tailed Student's t test analysis. (C) Immunoblot analysis of phospho-Smad3 (pSmad3) and Smad2/3, phospho-Akt and Akt, and phospho-Erk1/2 and Erk1/2 in WT, *Tg(Gasp-1)* and *Mstn* $^{-/-}$ primary myoblasts under proliferating conditions. Gapdh was used to ensure equal loadings. (D) Densitometric analysis of phosphorylated Smad3, Akt and Erk1/2 in WT, *Tg(Gasp-1)* and *Mstn* $^{-/-}$ primary myoblasts under proliferating conditions. **: p value < 0.05 ; **: p value < 0.01 ; ***: p value < 0.001.*

increased in *Tg(Gasp-1)* and *Mstn* $^{-/-}$ myoblasts compared to the WT, *Mstn* $^{-/-}$ myoblasts having the highest rate of phospho-Akt (Fig. 6C and 6D). Nevertheless, the analysis of Erk1/2 phosphorylation rate revealed that only *Tg(Gasp-1)* myoblasts had increased levels of activated Erk1/2 (Fig. 6C and 6D).

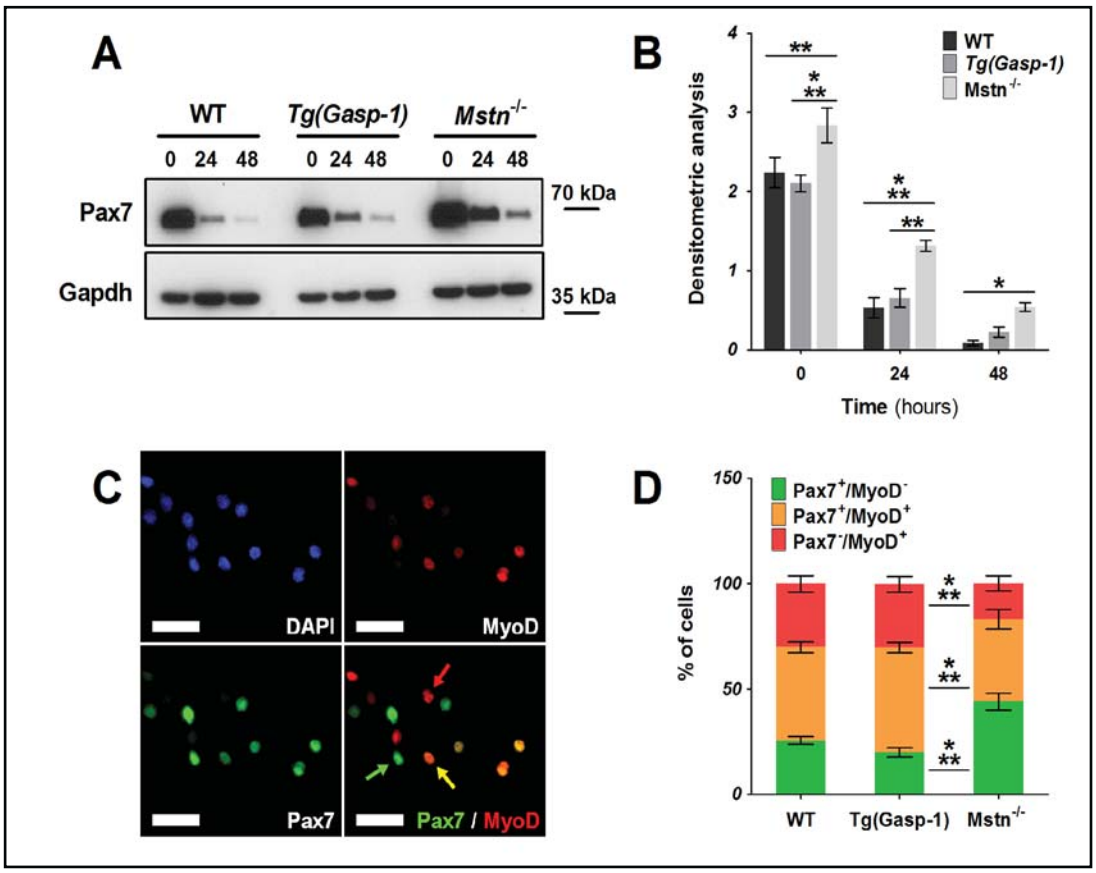

Fig. 7. Pax7, MyoD and double-stained immunofluorescence in wild-type compared to *Tg(Gasp-1)* primary cultures. (A) Western blotting comparative analysis of Pax7 in wild-type (WT), *Tg(Gasp-1)* and *Mstn* $^{-/-}$ primary myoblasts under proliferating conditions and at 24 h and 48 h of differentiation. (B) The graph represents the densitometric analysis of the relative protein levels of Pax7 normalized to Gapdh signals of three distinct experiments. Values are means ± SEM. Statistical significance was performed using by a two-way ANOVA when compared *Tg(Gasp-1)* and *Mstn* $^{-/-}$ with the WT. (C) Primary myoblasts were immunolocalized for Pax7 and MyoD proteins to analyze the proportion of Pax7^{+}/MyoD^{-} cells (green arrow), Pax7^{+}/MyoD^{+} cells (yellow arrow) and Pax7^{-}/MyoD^{+} (red arrow). Scale bars are 25 µm. (D) Percentage of undifferentiated Pax7^{+}/MyoD^{-} cells, committed Pax7^{+}/MyoD^{+} cells and differentiated Pax7^{-}/MyoD^{+} cells of WT, *Tg(Gasp-1)* and *Mstn* $^{-/-}$ cultures. Values are means ± SEM of four distinct experiments. ***: p value < 0.01 ; ***: p value < 0.001.*

Pax7 expression is deregulated in Tg(Gasp-1) myoblasts compared to the Mstn -/- myoblasts

Because Erk1/2 signaling pathway is involved in myostatin-induced Pax7 down-regulation [24], we analyzed the level of Pax7 in WT, *Tg(Gasp-1)* and *Mstn* $^{-/-}$ primary myoblasts with two independent experiments, namely Pax7 western blotting and immunofluorescence. Western blot analysis during the first 48 hours of differentiation revealed that Pax7 level had increased in *Mstn* $^{-/-}$ cells compared to the WT and *Tg(Gasp-1)* myoblasts. During proliferation, *Tg(Gasp-1)* myoblasts showed a slight decrease of Pax7 levels compared to the wild-type but it seemed to have increased during differentiation (Fig. 7A and 7B). Then, we analyzed the proportions of Pax7 and MyoD expressing cells between WT, *Tg(Gasp-1)* and *Mstn* $^{-/-}$ proliferating myoblasts by immunofluorescence (Fig. 7C). We obtained the same results for WT and *Tg(Gasp-1)* myoblasts, although *Tg(Gasp-1)* myoblast cultures had a slightly decreased proportion of undifferentiated Pax7^{+}/MyoD^{-} cells compared to the WT cultures (Fig. 7D). However, WT and *Tg(Gasp-1)* myoblasts were dramatically different from the *Mstn* $^{-/-}$ myoblasts which had the highest proportion of undifferentiated Pax7^{+}/MyoD^{-} cells and a reduced proportion of committed Pax7^{+}/MyoD^{+} cells and differentiated Pax7^{-}/

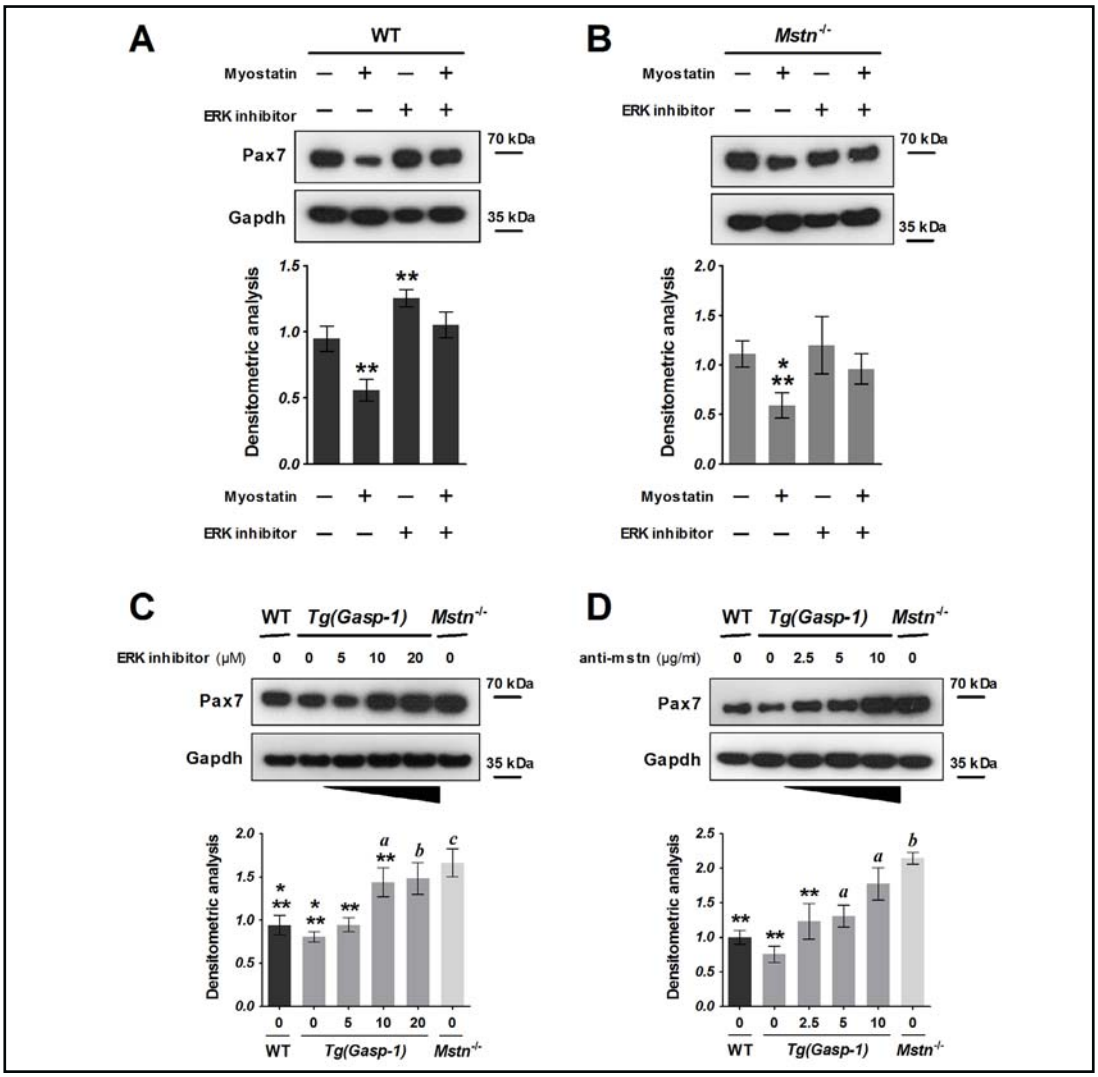

Fig. 8. Treatment of wild-type and *Tg(Gasp-1)* myoblasts by myostatin leads to deregulation of Pax7. (A) Western blot of Pax7 in wild-type (WT) proliferating myoblasts treated with (+) or without (-) recombinant myostatin protein (myostatin, 250 ng/ml), in the presence (+) or absence (-) of FR180204 (ERK inhibitor, 10 μM) for 16 h. Gapdh is used to ensure equal loading of samples. (B) Western blot of Pax7 in *Mstn* $^{-/-}$ proliferating myoblasts treated with (+) or without (-) recombinant myostatin protein (myostatin, 250 ng/ml), in the presence (+) or absence (-) of FR180204 (ERK inhibitor, 10 μM) for 16 h. (C) Western blotting comparative analysis of Pax7 in WT and *Mstn* $^{-/-}$ untreated myoblasts under proliferating conditions and *Tg(Gasp-1)* myoblasts treated with increasing concentrations of FR180204 (ERK inhibitor) for 16 h. (D) Western blotting comparative analysis of Pax7 in WT and *Mstn* $^{-/-}$ untreated myoblasts under proliferating conditions and *Tg(Gasp-1)* myoblasts treated with increasing concentrations of a neutralizing anti-myostatin antibody (anti-mstn) for 16 h. All graphs for panels A-D represent densitometric analysis of Pax7 expression normalized to Gapdh. Statistical significance was assessed by a Student's t test analysis when compared with the WT (***: p value < 0.01 ; ***: p value < 0.001*) or when compared to the *Mstn* $^{-/-}$ (*a: p value < 0.05 ; b: p value < 0.01 ; c: p value < 0.001*).

MyoD^{+} cells (Fig. 7D). Specifically, overexpression of *Gasp-1* seemed to result in reduced level of Pax7 when compared to the *Mstn* $^{-/-}$ cells, which may be responsible of a decrease of progenitor muscle cells in *Tg(Gasp-1)* mice compared to the *Mstn* $^{-/-}$ mice. Therefore, we hypothesized that deregulation of Pax7 could be related to the myostatin up-regulation and with the activation of Erk1/2 signaling pathway.

Up-regulation of myostatin in Tg(Gasp-1) myoblasts deregulates Pax7 expression

To verify this hypothesis, we first analyzed the ability of myostatin to regulate Pax7 through Erk1/2 pathway in WT and *Mstn* $^{-/-}$ myoblasts. When treated with a recombinant myostatin protein, both WT and *Mstn* $^{-/-}$ myoblasts showed a significant decrease of Pax7 levels (Fig. 8A and 8B). In contrast, treatment with ERK inhibitor increased Pax7 expression in WT myoblasts (Fig. 8A). Mainly, the combination of treatments by myostatin and ERK inhibitor prevented the decrease of Pax7 expression, confirming that myostatin signals through Erk1/2 pathway to regulate Pax7 (Fig. 8A). This phenomenon was also observed in *Mstn* $^{-/-}$ myoblasts, although a treatment with only ERK inhibitor didn't seemed to induce an increase of Pax7 in these cells (Fig. 8B). To determine whether Erk1/2 activation in *Tg(Gasp-1)* myoblasts could be related to Pax7 deregulation, we treated *Tg(Gasp-1)* myoblasts with increasing concentrations of ERK inhibitor (Fig. 8C). As described previously, untreated *Tg(Gasp-1)* myoblasts showed a slight decrease of Pax7 protein levels compared to WT myoblasts and *Mstn* $^{-/-}$ myoblasts had the highest Pax7 expression (Fig. 8C and 8D). As shown in Fig. 8C, increasing concentrations of ERK inhibitor enhanced Pax7 levels in *Tg(Gasp-1)* myoblasts, close to those of *Mstn* $^{-/-}$ myoblasts for the highest ERK inhibitor concentration, confirming that Erk1/2 activation in *Tg(Gasp-1)* myoblasts led to reduced Pax7 expression. Finally, we sought to determine whether neutralization of myostatin could increase Pax7 expression in *Tg(Gasp-1)* myoblasts. *Tg(Gasp-1)* myoblasts were treated with increasing concentrations of anti-myostatin antibodies for 16 hours (Fig. 8D). The more myostatin was neutralized, the more Pax7 expression was improved. Eventually, we showed that the highest concentrations of ERK inhibitor or anti-myostatin antibodies led to Pax7 proteins levels close to those observed in *Mstn* $^{-/-}$ myoblasts, suggesting that Pax7 deregulation in *Tg(Gasp-1)* myoblasts is related to myostatin up-regulation.

Discussion

Recently, we have generated different transgenic mouse lines that ubiquitously overexpress *Gasp-1*, called *Tg(Gasp-1)* lines, in order to better understand the role of *Gasp-1* during development [32]. In this paper, we investigated the cellular and molecular mechanisms deregulated by *Gasp-1* overexpression to provide a detailed muscle phenotype characterization. Previous studies have shown that GASP-1 is capable of binding both myostatin and GDF-11 to inhibit their canonical pathway *in vitro* [29, 38]. Mice lacking *Gasp-1* exhibit only a slight muscle atrophy without an axial skeletal phenotype. This reduced muscle mass was observed only in old *Gasp-1* $^{-/-}$ deficient mice (> 8 months). No significant differences between wild-type and mutant mice at 10 weeks of age was noted [39]. In contrast, *Tg(Gasp-1)* mice have an increased muscle mass due to hypertrophy, visible from 3 months of age. The delivery of an AAV encoding *Gasp-1* leads to myofiber hypertrophy in adult mice [17]. In our model, we confirmed that mice had an increased skeletal muscle mass due to an increase in myofiber size - hypertrophy equally affecting oxidative or glycolytic muscles - without a variation in the myofiber number (Fig. 1A and 1C). As this number in mice is established soon after birth [3], we hypothesized that the absence of hyperplasia in *Tg(Gasp-1)* mice may be due to the lack of *Gasp-1* overexpression during prenatal muscle development. Analysis of *Gasp-1* expression in E9.5 and E14.5 *Tg(Gasp-1)* embryos showed a 20-fold overexpression compared to the wild-type (Table 2). This result was confirmed by western blotting analysis of GASP-1 at these two stages of development (Fig. 5A). To go deeper in the regulation of muscle growth by *Gasp-1*, we investigated the signaling pathways in satellite cell-derived myoblasts from wild-type (WT) and *Tg(Gasp-1)* mice.

We first characterized the *Tg(Gasp-1)* myoblast phenotype, *i.e.* the proliferation and differentiation status. As shown in Fig. 2A and 2B, the *Tg(Gasp-1)* myoblasts proliferate faster than the WT, as previously described for the *Mstn* $^{-/-}$ primary myoblasts *in vitro* [40]. We also observed increased levels of Cdk2 and Cyclin D1, which cooperate to control the

cell cycle through phosphorylation and inactivation of the retinoblastoma (Rb) protein [41]. Cyclin-dependent kinase inhibitor (CKI) p21 level was decreased in the *Tg(Gasp-1)* myoblasts, confirming the cell cycle progression and the increase in proliferation rate [42]. We proposed that an increase in satellite cell-derived myoblasts proliferation could be associated with an increase in satellite cell number. However, no variation was found between 12-week-old wild-type and *Tg(Gasp-1)* mice (Fig. 1D and 1E). This result was not surprising, considering the recent analysis of satellite cell number in *Mstn* $^{-/-}$ mice [43]. There is no effect on activation and proliferation of satellite cells in *Mstn* $^{-/-}$ mice in adulthood [43, 44], although they have an increase in the progenitor cell number during embryonic development [45]. Since expression array analysis and ELISA revealed a significant overexpression of *Gasp-1* in *Tg(Gasp-1)* satellite cell-derived myoblasts (Fig. 4A and 4C), we could speculate that GASP-1 acts on the pool of satellite cells independently of myostatin. However, the absence of variation in number of satellite cells invalidates this hypothesis. The *Tg(Gasp-1)* myoblasts also differentiated faster than the wild-type cells, with an increase in both fusion index and myonuclei number (Fig. 3B and 3C). Increased protein levels of MyHC, myogenin and p21 (Fig. 3D and 3E), three major differentiation-related genes known to be down-regulated by myostatin [21], confirmed this enhanced differentiation, suggesting that *Gasp-1* overexpression promotes fusion, probably by inhibition of myostatin. The increase of both proliferation rate and myonuclei number in myotubes could be related to an enhancement of satellite cell activation and proliferation *in vivo*. The absence of variation in number of satellite cells at 12-week-old suggests that their activation and proliferation are taking place during the first 3 postnatal weeks and are leading to a higher myonuclear accretion consistent with the myofiber hypertrophy observed in *Tg(Gasp-1)* mice.

A comparison of activated signaling pathways between WT and *Tg(Gasp-1)* myoblasts revealed a decrease of Smad3 phosphorylation rate concomitant with an increase in phospho-Akt levels, correlating with the inhibition of myostatin (Fig. 6C and 6D) [22]. We also showed a global increase in the Akt/mTOR/p70S6K protein synthesis pathway (Fig. 6). All together, these results confirmed the activation of the pro-hypertrophic signaling pathway in *Tg(Gasp-1)* myoblasts.

Expression array analysis between WT and *Tg(Gasp-1)* myoblasts showed a significant up-regulation of *myostatin* and a down-regulation of *Igf-1* (Table 1, Fig. 4B). These results were previously observed in Smad3-null mice and led to decreased muscle mass and pronounced skeletal muscle atrophy [46]. The myostatin up-regulation was also observed at the protein level in primary *Tg(Gasp-1)* myoblasts and serum (Fig. 4F and 4H). In contrast to the Smad3-null mice, the secretion of GASP-1 in our transgenic model allows the inhibition of myostatin, even if this latter is more secreted. Thus, the *Tg(Gasp-1)* mice present an opposite phenotype of the Smad3-null mice – a myofiber hypertrophy – but intermediate to *Mstn* $^{-/-}$ one [8, 32, 46]. As shown in [47, 48], *myostatin* auto-regulates its expression by a feedback loop through Smad7 dependent mechanism, where Smad7 expression is stimulated by myostatin and dramatically reduces the myostatin-induced transcription. We demonstrate for the first time that the overexpression of an extracellular myostatin inhibitor leads to the up-regulation of myostatin through its feedback loop. Consistent with these data, we found a down-regulation of *Smad7*.

Expression array analysis also revealed an up-regulation of *Inhbb* in *Tg(Gasp-1)* myoblasts and mice compared to the wild-type (Tables 1 and 2). *Inhbb* is one of the four genes encoding inhibin-β subunits [49]. While inhibins are heterodimers of a unique alpha subunit and one of the various beta subunits, activins are homodimers or heterodimers of the various beta subunit isoforms. The activin B, which is a dimer of inhibin-βb subunits, contribute to the control of muscle development since the *Inhbb* $^{-/-}$ mice exhibit an increase of muscle mass [50]. The observed up-regulation could be involved in the intermediate phenotype of the *Tg(Gasp-1)* compared to *Mstn* $^{-/-}$ mice. However, in *Inhbb* $^{-/-}$ mice, only two muscles (pectoralis and triceps) showed a significant increase [50] while *Tg(Gasp-1)* mice exhibit a global increase of skeletal muscle mass [32]. Thus, the effect of *Inhbb* up-regulation is insubstantial compared to the *Mstn* up-regulation.

Surprisingly, expression array analysis revealed that *Fst* and *Fstl3* expressions (Table 1), two other myostatin and activin inhibitors [9], were down-regulated in overexpressing *Gasp-1* myoblasts, such as *Tgfβ1* known as an agonist factor of myostatin [51]. Moreover, expression array analysis in *Tg(Gasp-1)* mice compared to the wild-type revealed the same gene expression profiles. All these results suggest the existence of a gene expression regulatory network of TGF-β superfamily members and their inhibitors.

Finally, Taqman Low Density Array (TLDA) analysis also showed in primary *Tg(Gasp-1)* myoblasts and mice, a down-regulation of *Pax3* and *Pax7*, two major factors regulating muscle progenitor cell functions during embryogenesis and adulthood (Tables 1 and 2) [52]. In *Tg(Gasp-1)* myoblasts, we showed a significant decrease of Pax7 protein levels compared to the *Mstn* $^{-/-}$ myoblasts and a slight decrease compared to the WT (Fig. 7). As myostatin inhibits Pax7 expression through Erk1/2 signaling pathway and its inhibition leads to increased levels of Pax7 in primary myoblasts [24], we hypothesized that the *myostatin* up-regulation is associated with to this deregulation of Pax7. Inhibition of myostatin using neutralizing antibodies or inactivation of Erk1/2 signaling pathway rescue the Pax7 expression in *Tg(Gasp-1)* myoblasts (Fig. 8). At the highest inhibitor concentration, Pax7 expression in the *Tg(Gasp-1)* myoblasts is quite similar to *Mstn* $^{-/-}$ myoblasts. To exclude the action of other TGF-β on Pax7 regulation, we have determined Pax7 expression after inhibition of Erk1/2 signaling pathway in *Mstn* $^{-/-}$ myoblasts. We found no variation, suggesting that only myostatin regulates Pax7 expression *via* Erk1/2 pathway. In *Mstn* $^{-/-}$ mice, Matsakas et al. [44] and Manceau et al. [45] showed an increase in muscle progenitor Pax7^{+} cells during embryogenesis responsible for the hyperplasia observed in adult, underlying the importance of myostatin in the regulation of muscle progenitor pool . The decrease of Pax7 related to myostatin up-regulation in *Tg(Gasp-1)* myoblasts could be responsible for the absence of hyperplasia in *Tg(Gasp-1)* mice. Although, in embryonic stage, *Gasp-1* overexpression is weaker than in postnatal development and in adult, this is sufficient to induce *myostatin* up-regulation in *Tg(Gasp-1)* mice (Fig. 4) [32]. We propose this *myostatin* up-regulation counteracts *Gasp-1* effect during embryonic muscle development.

During embryogenesis, we suggest that myostatin acts preferentially through Erk1/2 signaling pathway to regulate Pax7 expression controlling the determination and the number of embryonic muscle progenitors. Thus, the absence of myostatin leads to the increase of muscle progenitors and consequently, an increase of myofiber number [45]. The Smad2/3 signaling pathway could regulate the size of myofibers during this step as *Mstn* $^{-/-}$ mice have a slight increase of their embryonic myofibers [44]. As we showed, overexpression of *Gasp-1* does not block the activation of Erk1/2 signaling pathway induced by myostatin, preventing hyperplasia in *Tg(Gasp-1)* mice. However, inhibition of Smad2/3 could be responsible for the hypertrophy observed in adult mice. In adulthood, myostatin could act preferentially through its canonical Smad2/3 signaling pathway to regulate cell proliferation, protein synthesis and myofiber size [23]. Absence of myostatin leads to increase of protein synthesis and therefore myofiber hypertrophy [23]. In *Tg(Gasp-1)* mice, we observed an intermediate hypertrophic phenotype due to a weaker inhibition of the Smad2/3 signaling pathway than in *Mstn* $^{-/-}$ mice.

Acknowledgments

This work was supported by the French National Institute of Agricultural Research and by the Limousin Regional Council. The authors thank Drs Pascal Maire and Fabrice Lalloué for their helpful scientific discussions.

Disclosure Statement

The authors have declared that no competing interests exist.

References

1 Berchtold MW, Brinkmeier H, Muntener M: Calcium ion in skeletal muscle: its crucial role for muscle function, plasticity, and disease. Physiol Rev 2000;80:1215-1265.
2 Charge SB, Rudnicki MA: Cellular and molecular regulation of muscle regeneration. Physiol Rev 2004;84:209-238.
3 Ontell M, Kozeka K: The organogenesis of murine striated muscle: a cytoarchitectural study. Am J Anat 1984;171:133-148.
4 White RB, Bierinx AS, Gnocchi VF, Zammit PS: Dynamics of muscle fibre growth during postnatal mouse development. BMC Dev Biol 2010;10:21.
5 Yin H, Price F, Rudnicki MA: Satellite cells and the muscle stem cell niche. Physiol Rev 2013;93:23-67.
6 Sandri M: Signaling in muscle atrophy and hypertrophy. Physiology (Bethesda) 2008;23:160-170.
7 Schiaffino S, Dyar KA, Ciciliot S, Blaauw B, Sandri M: Mechanisms regulating skeletal muscle growth and atrophy. FEBS J 2013;280:4294-4314.
8 McPherron AC, Lawler AM, Lee SJ: Regulation of skeletal muscle mass in mice by a new TGF-beta superfamily member. Nature 1997;387:83-90.
9 Lee SJ: Extracellular Regulation of Myostatin: A Molecular Rheostat for Muscle Mass. Immunol Endocr Metab Agents Med Chem 2010;10:183-194.
10 Girgenrath S, Song K, Whittemore LA: Loss of myostatin expression alters fiber-type distribution and expression of myosin heavy chain isoforms in slow- and fast-type skeletal muscle. Muscle Nerve 2005;31:34-40.
11 Lin J, Arnold HB, Della-Fera MA, Azain MJ, Hartzell DL, Baile CA: Myostatin knockout in mice increases myogenesis and decreases adipogenesis. Biochem Biophys Res Commun 2002;291:701-706.
12 Mosher DS, Quignon P, Bustamante CD, Sutter NB, Mellersh CS, Parker HG, Ostrander EA: A mutation in the myostatin gene increases muscle mass and enhances racing performance in heterozygote dogs. PLoS Genet 2007;3:e79.
13 Schuelke M, Wagner KR, Stolz LE, Hubner C, Riebel T, Komen W, Braun T, Tobin JF, Lee SJ: Myostatin mutation associated with gross muscle hypertrophy in a child. N Engl J Med 2004;350:2682-2688.
14 Karim L, Coppieters W, Grobet L, Valentini A, Georges M: Convenient genotyping of six myostatin mutations causing double-muscling in cattle using a multiplex oligonucleotide ligation assay. Anim Genet 2000;31:396-399.
15 Clop A, Marcq F, Takeda H, Pirottin D, Tordoir X, Bibe B, Bouix J, Caiment F, Elsen JM, Eychenne F, Larzul C, Laville E, Meish F, Milenkovic D, Tobin J, Charlier C, Georges M: A mutation creating a potential illegitimate microRNA target site in the myostatin gene affects muscularity in sheep. Nat Genet 2006;38:813-818.
16 Grobet L, Pirottin D, Farnir F, Poncelet D, Royo LJ, Brouwers B, Christians E, Desmecht D, Coignoul F, Kahn R, Georges M: Modulating skeletal muscle mass by postnatal, muscle-specific inactivation of the myostatin gene. Genesis 2003;35:227-238.
17 Haidet AM, Rizo L, Handy C, Umapathi P, Eagle A, Shilling C, Boue D, Martin PT, Sahenk Z, Mendell JR, Kaspar BK: Long-term enhancement of skeletal muscle mass and strength by single gene administration of myostatin inhibitors. Proc Natl Acad Sci U S A 2008;105:4318-4322.
18 Bogdanovich S, Perkins KJ, Krag TO, Whittemore LA, Khurana TS: Myostatin propeptide-mediated amelioration of dystrophic pathophysiology. FASEB J 2005;19:543-549.
19 Whittemore LA, Song K, Li X, Aghajanian J, Davies M, Girgenrath S, Hill JJ, Jalenak M, Kelley P, Knight A, Maylor R, O'Hara D, Pearson A, Quazi A, Ryerson S, Tan XY, Tomkinson KN, Veldman GM, Widom A, Wright JF, Wudyka S, Zhao L, Wolfman NM: Inhibition of myostatin in adult mice increases skeletal muscle mass and strength. Biochem Biophys Res Commun 2003;300:965-971.
20 Thomas M, Langley B, Berry C, Sharma M, Kirk S, Bass J, Kambadur R: Myostatin, a negative regulator of muscle growth, functions by inhibiting myoblast proliferation. J Biol Chem 2000;275:40235-40243.
21 Langley B, Thomas M, Bishop A, Sharma M, Gilmour S, Kambadur R: Myostatin inhibits myoblast differentiation by down-regulating MyoD expression. J Biol Chem 2002;277:49831-49840.
22 Trendelenburg AU, Meyer A, Rohner D, Boyle J, Hatakeyama S, Glass DJ: Myostatin reduces Akt/TORC1/p70S6K signaling, inhibiting myoblast differentiation and myotube size. Am J Physiol Cell Physiol 2009;296:C1258-1270.
23 Sartori R, Milan G, Patron M, Mammucari C, Blaauw B, Abraham R, Sandri M: Smad2 and 3 transcription factors control muscle mass in adulthood. Am J Physiol Cell Physiol 2009;296:C1248-1257.
24 McFarlane C, Hennebry A, Thomas M, Plummer E, Ling N, Sharma M, Kambadur R: Myostatin signals through Pax7 to regulate satellite cell self-renewal. Exp Cell Res 2008;314:317-329.
25 Yang W, Chen Y, Zhang Y, Wang X, Yang N, Zhu D: Extracellular signal-regulated kinase 1/2 mitogen-activated protein kinase pathway is involved in myostatin-regulated differentiation repression. Cancer Res

2006;66:1320-1326.
26 Massague J, Chen YG: Controlling TGF-beta signaling. Genes Dev 2000;14:627-644.
27 Carnac G, Vernus B, Bonnieu A: Myostatin in the pathophysiology of skeletal muscle. Curr Genomics 2007;8:415-422.
28 Hill JJ, Qiu Y, Hewick RM, Wolfman NM: Regulation of myostatin in vivo by growth and differentiation factor-associated serum protein-1: a novel protein with protease inhibitor and follistatin domains. Mol Endocrinol 2003;17:1144-1154.
29 Brun C, Monestier O, Legardinier S, Maftah A, Blanquet V: Murine GASP-1 N-glycosylation is not essential for its activity on C2C12 myogenic cells but alters its secretion. Cell Physiol Biochem 2012;30:791-804.
30 Kondas K, Szlama G, Trexler M, Patthy L: Both WFIKKN1 and WFIKKN2 have high affinity for growth and differentiation factors 8 and 11. J Biol Chem 2008;283:23677-23684.
31 Szlama G, Kondas K, Trexler M, Patthy L: WFIKKN1 and WFIKKN2 bind growth factors TGFbeta1, BMP2 and BMP4 but do not inhibit their signalling activity. FEBS J 2010;277:5040-5050.
32 Monestier O, Brun C, Heu K, Passet B, Malhouroux M, Magnol L, Vilotte JL, Blanquet V: Ubiquitous Gasp1 overexpression in mice leads mainly to a hypermuscular phenotype. BMC Genomics 2012;13:541.
33 Oliver MH, Harrison NK, Bishop JE, Cole PJ, Laurent GJ: A rapid and convenient assay for counting cells cultured in microwell plates: application for assessment of growth factors. J Cell Sci 1989;92 (Pt 3):513-518.
34 Musaro A, McCullagh K, Paul A, Houghton L, Dobrowolny G, Molinaro M, Barton ER, Sweeney HL, Rosenthal N: Localized Igf-1 transgene expression sustains hypertrophy and regeneration in senescent skeletal muscle. Nat Genet 2001;27:195-200.
35 Biressi S, Molinaro M, Cossu G: Cellular heterogeneity during vertebrate skeletal muscle development. Dev Biol 2007;308:281-293.
36 Dodd SL, Hain B, Senf SM, Judge AR: Hsp27 inhibits IKKbeta-induced NF-kappaB activity and skeletal muscle atrophy. FASEB J 2009;23:3415-3423.
37 Senf SM, Dodd SL, McClung JM, Judge AR: Hsp70 overexpression inhibits NF-kappaB and Foxo3a transcriptional activities and prevents skeletal muscle atrophy. FASEB J 2008;22:3836-3845.
38 Bonala S, Lokireddy S, Arigela H, Teng S, Wahli W, Sharma M, McFarlane C, Kambadur R: Peroxisome proliferator-activated receptor beta/delta induces myogenesis by modulating myostatin activity. J Biol Chem 2012;287:12935-12951.
39 Lee YS, Lee SJ: Regulation of GDF-11 and myostatin activity by GASP-1 and GASP-2. Proc Natl Acad Sci U S A 2013;10.1073/pnas.1309907110
40 McCroskery S, Thomas M, Maxwell L, Sharma M, Kambadur R: Myostatin negatively regulates satellite cell activation and self-renewal. J Cell Biol 2003;162:1135-1147.
41 Guo K, Walsh K: Inhibition of myogenesis by multiple cyclin-Cdk complexes. Coordinate regulation of myogenesis and cell cycle activity at the level of E2F. J Biol Chem 1997;272:791-797.
42 Sherr CJ, Roberts JM: CDK inhibitors: positive and negative regulators of G1-phase progression. Genes Dev 1999;13:1501-1512.
43 Wang Q, McPherron AC: Myostatin inhibition induces muscle fibre hypertrophy prior to satellite cell activation. J Physiol 2012;590:2151-2165.
44 Matsakas A, Otto A, Elashry MI, Brown SC, Patel K: Altered primary and secondary myogenesis in the myostatin-null mouse. Rejuvenation Res 2010;13:717-727.
45 Manceau M, Gros J, Savage K, Thome V, McPherron A, Paterson B, Marcelle C: Myostatin promotes the terminal differentiation of embryonic muscle progenitors. Genes Dev 2008;22:668-681.
46 Ge X, McFarlane C, Vajjala A, Lokireddy S, Ng ZH, Tan CK, Tan NS, Wahli W, Sharma M, Kambadur R: Smad3 signaling is required for satellite cell function and myogenic differentiation of myoblasts. Cell Res 2011;21:1591-1604.
47 Forbes D, Jackman M, Bishop A, Thomas M, Kambadur R, Sharma M: Myostatin auto-regulates its expression by feedback loop through Smad7 dependent mechanism. J Cell Physiol 2006;206:264-272.
48 Zhu X, Topouzis S, Liang LF, Stotish RL: Myostatin signaling through Smad2, Smad3 and Smad4 is regulated by the inhibitory Smad7 by a negative feedback mechanism. Cytokine 2004;26:262-272.
49 Chang H, Brown CW, Matzuk MM: Genetic analysis of the mammalian transforming growth factor-beta superfamily. Endocr Rev 2002;23:787-823.
50 Lee SJ, Lee YS, Zimmers TA, Soleimani A, Matzuk MM, Tsuchida K, Cohn RD, Barton ER: Regulation of muscle mass by follistatin and activins. Mol Endocrinol 2010;24:1998-2008.
51 Allen RE, Boxhorn LK: Inhibition of skeletal muscle satellite cell differentiation by transforming growth factor-beta. J Cell Physiol 1987;133:567-572.
52 Buckingham M, Relaix F: The role of Pax genes in the development of tissues and organs: Pax3 and Pax7 regulate muscle progenitor cell functions. Annu Rev Cell Dev Biol 2007;23:645-673.